

# HII-DPO: Eliminate Hallucination via Accurate Hallucination-Inducing Counterfactual Images

Yilin Yang<sup>1</sup> Zhenghui Guo<sup>1</sup> Yuke Wang<sup>2</sup> Omprakash Gnawali<sup>1</sup> Sheng Di<sup>3</sup> Chengming Zhang<sup>1†</sup>

## Abstract

Large Vision-Language Models (VLMs) have achieved remarkable success across diverse multimodal tasks but remain vulnerable to hallucinations rooted in inherent language bias. Despite recent progress, existing hallucination mitigation methods often overlook the underlying hallucination patterns driven by language bias. In this work, we design a novel pipeline to accurately synthesize Hallucination-Inducing Images (HIIs). Using synthesized HIIs, we reveal a consistent scene-conditioned hallucination pattern: models tend to mention objects that are highly typical of the scene even when visual evidence is removed. To quantify the susceptibility of VLMs to this hallucination pattern, we establish the Masked-Object-Hallucination (MOH) benchmark to rigorously evaluate existing state-of-the-art alignment frameworks. Finally, we leverage HIIs to construct high-quality preference datasets for fine-grained alignment. Experimental results demonstrate that our approach effectively mitigates hallucinations while preserving general model capabilities. Specifically, our method achieves up to a 38% improvement over the current state-of-the-art on standard hallucination benchmarks.

## 1. Introduction

Large Vision-Language Models (VLMs) demonstrate remarkable capabilities in jointly perceiving and reasoning over images and text, facilitating applications in assistive technologies, education, medical imaging, and industrial inspection. Despite this outstanding progress, modern VLMs are still prone to hallucinations, producing fluent yet visually incorrect content or misaligning visual evidence with textual outputs (Rohrbach et al., 2018; Zhao et al., 2023; Xiong et al., 2024). Such inconsistency drastically undermines the

trustworthiness of AI systems and hinders the widespread applications of VLMs.

Recent research (Wang et al., 2024a; Xing et al., 2025; Chen et al., 2025; Zadeh et al., 2025; Zhou et al., 2024b;a) indicates that VLMs are prone to modality bias, a phenomenon where generation is disproportionately guided by linguistic priors at the expense of visual evidence. For example, a VLM may instinctively generate the term “sink” following the mention of “kitchen”, or a “keyboard” following the mention of an “office”, relying on textual co-occurrences learned during training. Consequently, visual details are overlooked, resulting in severe hallucinations and compromised model trustworthiness. This issue stems primarily from an architectural imbalance in current VLMs, where the Large Language Model (LLM) component dominates the visual encoder. Consequently, VLMs inevitably rely on the linguistic priors, rather than grounding their responses in visual evidence. This phenomenon is referred to as **Language Bias** or **Language Prior**.

These deficiencies have motivated a shift toward Direct Preference Optimization (DPO) (Rafailov et al., 2024; Wang et al., 2024a; Xing et al., 2025; Zhou et al., 2024a; Zhang et al., 2025) which is emerging as a crucial approach to mitigate language bias and enhance visual faithfulness. Specifically, mDPO (Wang et al., 2024a) pioneered the paradigm of utilizing contrastive visual signals for preference optimization—a framework we define as Vision-Contrastive Alignment (VCA). VCA-based methods compel VLMs to prioritize visual modalities by leveraging visual contrastive preferences. However, current VCA-based approaches are hindered by three critical limitations. First, these implementations suffer from semantic ambiguity. The chosen responses often retain semantic details that remain partially grounded in the rejected visual inputs, resulting in a coarse-grained alignment signal that lacks the resolution to distinguish specific object-level absences. Second, the construction of rejected images via stochastic processes, such as random cropping or similarity-based retrieval, is fundamentally insufficient to generate “hard” negative samples, as it often fails to preserve the scene context necessary to trigger linguistic priors. Third, existing VCA-based frameworks fail to leverage negative images to construct chosen and

<sup>1</sup>University of Houston <sup>2</sup>Rice University <sup>3</sup>Argonne National Laboratory. Correspondence to: Chengming Zhang <czhang59@central.uh.edu>.

rejected responses for preference alignment. Consequently, VLMs do not learn a deeper understanding of the negative images, leading to suboptimal performance on various benchmarks. Therefore, it remains challenging to generate precise, “hard” counterfactual samples or preference datasets that can effectively decouple linguistic priors from visual evidence during preference alignment.

**Our Observation.** We revisit object hallucination from the perspective of **scene-object co-occurrence**, i.e., the tendency for certain objects to frequently appear in particular scenes. Such co-occurrence bias can shape the model’s language prior in DDG. For instance, VLMs often mention “*sink*” in the kitchen, “*stop sign*” at crossroads, or “*train*” on railways, as these objects are highly probable given the surrounding context. To investigate this effect, we construct counterfactual images by deliberately removing salient objects from the input and then prompt VLMs to perform DDG. We find that VLMs across a range of model scales and architectures still *falsey assert the presence* of the removed objects even when there is no supporting visual evidence. We refer to this failure mode as **scene-conditioned hallucination**: hallucinations conditioned on the remaining scene context (in the image or the textual prompt) after object removed in the image, in which a model’s predictions are strongly influenced by scene-object co-occurrence priors and thus can override grounded visual cues under counterfactual inputs. This phenomenon may be partially explained by the high frequency of co-occurrence between specific scenarios and objects in SFT corpora, which can reinforce such priors. However, existing approaches have not provided an effective way to quantitatively evaluate hallucination conditioned by the scene, or a principled strategy to mitigate it.

**Our Contributions.** To investigate and quantify the scene-conditioned hallucination pattern, we introduce a systematic pipeline to synthesize accurate Hallucination-Inducing Images (HIIs). By strategically removing salient objects from natural images, we curate a set of high-quality, accurate counterfactual samples, where models are highly prone to hallucinating missing entities due to rooted linguistic bias. Utilizing these counterfactual images, we construct the Masked-Object-Hallucination (MOH) benchmark. This novel evaluation framework assesses a model’s resilience when confronted with counterfactual images. This helps us to quantitatively analyze how existing state-of-the-art (SOTA) alignment frameworks mitigate this specific hallucination pattern. Finally, we propose HII-DPO, a novel data construction and preference alignment pipeline, designed to decouple language bias from visual grounding. Utilizing HIIs, HII-DPO synthesizes fine-grained preference pairs that explicitly guide the Direct Preference Optimization (DPO) process, effectively teaching models to remain faithful to visual inputs rather than relying on stereotypical scene-object co-occurrences.

We evaluate current SOTA methods on our newly proposed MOH benchmark, providing a rigorous quantitative analysis of hallucination rates under counterfactual scenarios. We also conduct extensive experiments on multiple benchmarks using HII-DPO. Specifically, our method achieves up to a 38% improvement over existing SOTA methods and reduces the hallucination rate by up to 92% compared to baseline models on the standard hallucination benchmarks (Rohrbach et al., 2018; Wang et al., 2024b). Crucially, this gain does not come at the cost of general capabilities, as our model maintains robust performance on standard VQA tasks (Goyal et al., 2017a; Singh et al., 2019a; Lu et al., 2022; Yu et al., 2023).

In summary, our contributions are four-fold:

- We devise a systematic pipeline to synthesize accurate HIIs. These counterfactual images effectively induce scene-conditioned hallucinations, providing a high-quality diagnostic tool to expose the linguistic bias rooted in VLMs.
- To quantitatively evaluate the scene-conditioned hallucination pattern, we curate the MOH benchmark. By rigorously testing existing approaches, we empirically demonstrate the prevalence of scene-object stereotypical predictions and provide a quantitative analysis of VLMs’ susceptibility to scene-conditioned hallucination.
- Leveraging HIIs, we propose a novel data construction and preference alignment framework, HII-DPO. Utilizing fine-grained preference pairs with shared prefixes, our pipeline effectively mitigates scene-conditioned hallucinations by teaching models to prioritize visual grounding over biased linguistic heuristics.
- Extensive experimental results confirm that our approach establishes a new state-of-the-art across multiple hallucination benchmarks while preserving general multimodal capabilities.

## 2. Preliminaries

In this section, we will briefly introduce the background of VLMs and direct preference optimization, serving as the theoretical basis for our approach.

### 2.1. Large Vision Language Model

Large Vision-Language Models (VLMs) aim to unify visual and linguistic understanding by extending large language models (LLMs) with visual perception modules. Typically, a VLM consists of three major components: a *vision encoder*, a *multimodal projector*, and a *language decoder*. The vision encoder (e.g., CLIP (Radford et al., 2021), ViT (Dosovitskiy et al., 2021), or SigLIP (Zhai et al., 2023)) extracts

dense visual representations from the input image. The multimodal projector aligns the visual embeddings with the token embedding space of the language model, enabling cross-modal interactions. Finally, the language decoder (e.g., LLaMA (Touvron et al., 2023), Vicuna (Chiang et al., 2023), or Qwen2 (Yang et al., 2024)) autoregressively generates textual outputs conditioned on both the visual context and the input instruction.

## 2.2. Direct Preference Optimization

In order to improve performance of VLMs, Direct Preference Optimization (DPO) (Rafailov et al., 2023) and its diverse variants (Wang et al., 2024a; Xing et al., 2025; Zhou et al., 2024a; Zhang et al., 2025) have been shown to be an efficient fine-tuning method that requires minimal additional computational resources. For the standard DPO in a multimodal setting, a preference pair is defined as  $\mathcal{D} = \{x, v, y^+, y^-\}$ , where  $y^-$  and  $y^+$  represent preferred and dispreferred responses, respectively.  $x$  is the input prompt and  $v$  is the visual signal input. DPO is based on Bradley-Terry Model (BT) (Bradley & Terry, 1952). The objective of the BT model is to maximize the likelihood of the observed preference pairs, i.e., the probability that the preferred response is ranked higher than the dispreferred one:

$$p(y^+ \succ y^-) = \sigma(r(x, v, y^+) - r(x, v, y^-)) \quad (1)$$

In the DPO scenario,  $r(x, v, y)$  is defined as the implicit reward of a specific preference data tuple  $(x, v, y)$ . For a single preference tuple  $(x, v, y)$ :

$$r(x, v, y) = \beta \cdot \log \frac{\pi_\theta(y|x, v)}{\pi_{\text{ref}}(y|x, v)} \quad (2)$$

Here  $\pi_{\text{ref}}$  is denoted as the reference model.  $\pi_\theta$  is the policy model. Finally, Equation 1 can be reformulated in the form of a maximum-likelihood objective computed over the entire training dataset:

$$\mathcal{L}_{\text{DPO}} = -\log \sigma \left( \beta \log \frac{\pi_\theta(y^+|x, v)}{\pi_{\text{ref}}(y^+|x, v)} - \beta \log \frac{\pi_\theta(y^-|x, v)}{\pi_{\text{ref}}(y^-|x, v)} \right). \quad (3)$$

Recent work (Xing et al., 2025; Peng et al., 2025; Li et al., 2024; He et al., 2024; Yu et al., 2025) focuses on generating high-quality preference data for DPO to achieve the proper alignment between vision and language.

## 3. Method

### 3.1. Overview

We present the overview of our framework in Figure 1. First, we propose a new pipeline for synthesizing HIIIs based on our observations about language priors. Second, we design

a new benchmark based on the counterfactual images to evaluate whether models can overcome language priors and scene-conditioned biases to make correct object-existence judgments. Finally, to address this failure mode, we design a preference-data construction pipeline which leverages HIIIs to build high-quality datasets without relying on any proprietary model (e.g., GPT-4 (Achiam et al., 2023)).

### 3.2. Hallucination-Inducing Images (HIIIs) Synthesis

In this section, we describe the pipeline Figure 2 designed to synthesize and select Hallucination-Inducing Images (HIIIs). To support open-vocabulary detection, we utilize GroundingDINO (Liu et al., 2024) to verify the presence of entities within an image. However, since the space of potential object categories is prohibitively large, we constrain our research scope to the 80 MS-COCO categories to ensure reproducibility and detection precision.

**Entity Detection.** Following the methodology of (Rohrbach et al., 2018), we utilize a synonym dictionary to map detected entities—specifically those recognized within the dictionary—onto 80 target classes. Candidate objects are then identified for each class. To ensure robust detection, we only retain target classes whose confidence scores exceed a predefined threshold (e.g., 0.5). More examples of the synonym dictionary are presented in Appendix C.

**Iterative Masking.** Next, a targeted masking strategy is applied to each filtered class. To mitigate issues related to incomplete occlusion or detection gaps, we implement an iterative masking procedure: for a given (image, class) pair, we perform successive detection-and-masking cycles until the target entity is fully occluded. Consequently, a single source image may yield multiple masked variants.

**Model-Specific HII Filtering.** Finally, the synthesized masked images are utilized to task the target VLMs to perform Detailed Description Generation (DDG) tasks. To ensure the robustness of our findings, we employ sampling-based decoding to generate 10 independent responses for each masked image. We then extract the object entities mentioned in these responses using language toolkits (e.g., nltk). An image is categorized as an HII specific to a model if that model asserts the presence of the successfully masked object in a majority of its responses (i.e., at least 5 out of 10). By requiring this frequency threshold, we filter out stochastic noise and ensure that the identified hallucinations are consistent model-specific behaviors directly tied to the absence of visual evidence.

### 3.3. The Masked-Object-Hallucination Benchmark

Using the HIIIs synthesis pipeline, we curate the **Masked-Object Hallucination Benchmark (MOH)** in Figure 3. We collect model-specific HIIIs from a diverse set of VLMs, including the Qwen-VL family (Wang et al., 2024c; Bai et al.,

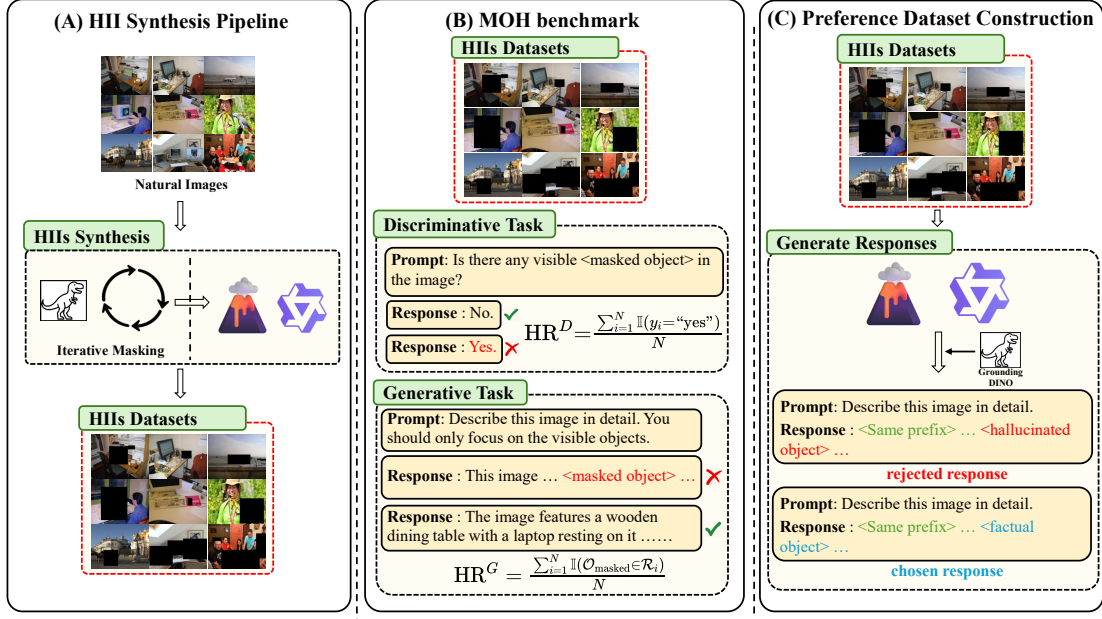


Figure 1. Overview of our framework. (A) Synthesize HII using GroundingDINO and open-source VLMs. (B) Construct MOH benchmark to quantitatively evaluate the scene-conditioned hallucination pattern. (C) Generate preference dataset using HII.

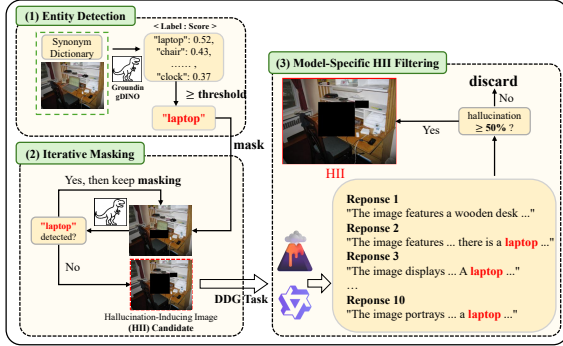


Figure 2. Overview of the HII Synthesis Pipeline. (1): Potential entities are identified via GroundingDINO based on a predefined synonym dictionary. (2): A detection-masking cycle is employed to achieve complete occlusion of the target entity, yielding HII candidates. (3) Task the target VLM to perform DDG and retain only those images with  $HR \geq 50\%$ .

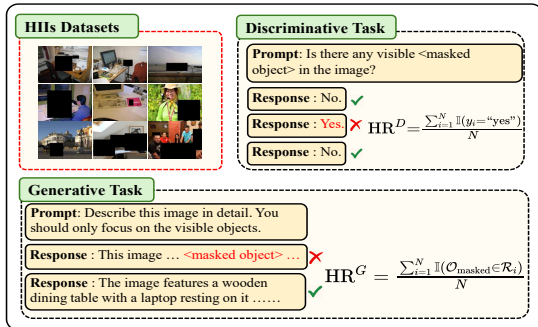


Figure 3. Masked-Object-Hallucination Benchmark.

2025; 2023) and LLaVA-1.5 (Liu et al., 2023) To identify the most challenging samples, we take the **intersection** of these model-specific HII datasets, selecting images that consistently trigger hallucinations across all tested architectures to form our core evaluation set.

**Evaluation Tasks.** To evaluate VLM performance comprehensively, we design two distinct evaluation paradigms:

- **Discriminative Probing:** We present the model with a direct query: “*Is there any visible [masked object] in the image?*”. A “No” response is categorized as correct, while a “Yes” indicates a hallucination.
- **Generative Description:** We task the model with DDG and extract entities from the generated text. Specifically, we identify all mentioned entities and normalize them using our synonym dictionary. A hallucination is recorded if the model explicitly claims the presence of the masked object.

**Scene Taxonomy.** Since our MOH benchmark comprises the intersection of HII identified by models with diverse scales and architectures, it serves as a robust instrument for investigating universal hallucination patterns. To further uncover these underlying contextual drivers, we manually partition the benchmark into ten distinct environmental domains: *Waterfront*, *Street*, *Railroad*, *Office*, *Dining Room*, *Kitchen*, *Bathroom*, *Ski Resort*, *Other Outdoor*, and *Other Indoor*. This taxonomy facilitates a granular analysis of the scene-conditioned hallucination pattern. We provide quantitative statistics on scene-object co-occurrence in sub-section 4.3.

**Metric** Unlike the standard  $\text{CHAIR}_i$  metric (Rohrbach et al., 2018), which can be sensitive to the frequency of correctly identified objects and prone to inflation via redundant mentions, we utilize the **Hallucination Rate (HR)** as our primary evaluation metric. For the generative task, we define HR as the ratio of model responses containing the masked object to the total number of generated responses:

$$\text{HR}^G = \frac{\sum_{i=1}^N \mathbb{I}(\mathcal{O}_{\text{masked}} \in \mathcal{R}_i)}{N} \quad (4)$$

where  $N$  denotes the total number of evaluation responses,  $\mathcal{R}_i$  represents the set of objects extracted from the  $i$ -th response  $y_i$ , and  $\mathbb{I}(\cdot)$  is the indicator function that outputs 1 if the masked object  $\mathcal{O}_{\text{masked}}$  is detected in the response. Similarly, we can define HR for the discriminative task as follows:

$$\text{HR}^D = \frac{\sum_{i=1}^N \mathbb{I}(y_i = \text{"yes"})}{N} \quad (5)$$

Since our benchmark specifically focuses on the “negative existence” of a known masked object, HR provides a more direct and precise measure of a VLM’s susceptibility to hallucinatory claims without the noise introduced by the density of other present objects.

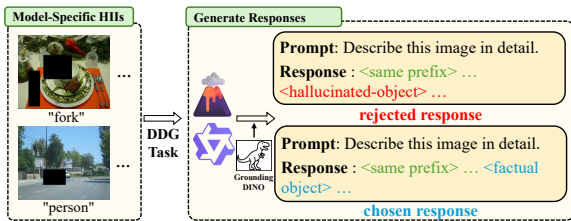


**Figure 4. Preference Dataset Generation.** Utilizing curated model-specific HII datasets, we construct contrastive response pairs where the *chosen* and *rejected* responses share an identical prefix. Verified by GroundingDINO, the rejected responses contain the hallucinated objects, whereas the chosen response describes only factual entities.

### 3.4. Preference Dataset Construction for DPO

To further mitigate hallucinatory behaviors, we leverage the curated model-specific HII datasets to construct a preference dataset for Direct Preference Optimization (DPO) as shown in Figure 4. To ensure the preference pairs remain within the model’s internal distribution, we directly utilize the target VLMs to generate both chosen and rejected responses. A synonym dictionary is employed to detect potential entity words within the generated responses as introduced in subsection 3.3. Subsequently, **GroundingDINO** (Liu et al., 2024) is utilized to verify the physical presence of these entities in the corresponding image. If GroundingDINO fails to detect the extracted entity, the response is confirmed to contain a hallucination and is categorized as “rejected”.

However, standard DPO on full-length responses often introduces noise, as a “rejected” response may still contain significant factual information. Drawing inspiration from SENTINEL (Peng et al., 2025), we adopt a sentence-by-sentence generation strategy to enforce fine-grained alignment. Specifically, we identify pairs where the chosen and rejected responses share an identical prefix and diverge only at a specific sentence. In these pairs, the “chosen sentence” is factually accurate, while the “rejected sentence” contains at least one hallucinated physical entity. By optimizing on these minimal contrastive pairs, we ensure that the DPO training focuses strictly on the hallucinated sentences, effectively preventing the VLM from learning from noisy supervision signals while preserving its underlying factual knowledge. By integrating Direct Preference Optimization (DPO) with the concept of Hallucination-Inducing Images (HII), we propose **HII-DPO**, which is formulated as follows:

$$\mathcal{L}(\theta) = -\mathbb{E}_{(\mathbf{x}, \mathbf{v}', \mathbf{y}^+, \mathbf{y}^-) \sim \mathcal{D}} \left[ \log \sigma \left( \beta \log \frac{\pi_{\theta}(\mathbf{y}^+ | \mathbf{x}, \mathbf{v}')}{\pi_{\text{ref}}(\mathbf{y}^+ | \mathbf{x}, \mathbf{v}')} \right. \right. \\ \left. \left. - \beta \log \frac{\pi_{\theta}(\mathbf{y}^- | \mathbf{x}, \mathbf{v}')}{\pi_{\text{ref}}(\mathbf{y}^- | \mathbf{x}, \mathbf{v}')} \right) \right] \quad (6)$$

Where  $\mathbf{y}^+$  and  $\mathbf{y}^-$  represent the generated chosen response and rejected response, respectively.  $\mathbf{x}$  denotes the context or prompt, and  $\mathbf{v}'$  refers to the Hallucination-Inducing Image (HII). The HII is defined as  $\mathbf{v}' = \mathbf{v} - \mathbf{o}$ , where  $\mathbf{v}$  is the original natural image and  $\mathbf{o}$  represents the specific object that has been removed (or masked out). We present a mathematical explanation about why HII are effective for preference alignment in mitigating object hallucination in Appendix A.

## 4. Experiments

In this section, we conduct extensive experiments to demonstrate the superiority of HII-DPO. Our method achieves state-of-the-art performance across multiple hallucination benchmarks while maintaining competitive general capabilities. We first detail the experimental setup in subsection 4.1, followed by the presentation of main results in subsection 4.2. In subsection 4.3, we evaluate existing approaches on our proposed MOH benchmark to verify the scene-conditioned hallucination pattern and analyze the correlation between scenes and objects. Furthermore, we provide an ablation study in subsection 4.4. Finally, inspired by mDPO (Wang et al., 2024a), we incorporate visual contrastive signals for preference alignment and compare our approach with mDPO and Re-Align (Xing et al., 2025), highlighting potential limitations of this training paradigm.

### 4.1. Experimental Setups

**Dataset** Following the HII Synthesis Pipeline in (Figure 2), we curated a final set of approximately 800 HII

to constitute the MOH benchmark. For the preference dataset, we identified model-specific HIIIs tailored to various architectures and scales, subsequently constructing chosen-rejected preference pairs using these HIIIs. To prevent data leakage, we utilized distinct sets of base images for the synthesis of HIIIs which are for the MOH benchmark and the preference dataset construction, respectively. Specifically, for MOH, we chose COCO2014 (Lin et al., 2015) as the base dataset. The preference dataset was synthesized based on 8,000 natural images sampled from Visual Genome (Krishna et al., 2017). To verify the physical existence of entities mentioned in the generated responses, we employed GroundingDINO (Liu et al., 2024) as our open-vocabulary detection model.

**Evaluation Benchmarks.** For hallucination benchmarks, we use Object Hallucination (Rohrbach et al., 2018), Amber (Wang et al., 2024b) and HallusionBench (Guan et al., 2024). For general VQA benchmarks, we utilize ScienceQA (Lu et al., 2022), TextVQA (Singh et al., 2019b), VQAv2 (Goyal et al., 2017b) and MM-Vet (Yu et al., 2023).

**Baseline Approaches.** Following the standard configurations established in recent studies, we adopt LLaVA-v1.5-7B and 13B (Liu et al., 2023) as the base architectures for our experiments. We conduct comprehensive comparisons between our approach and several state-of-the-art VLM alignment frameworks including Re-Align (Xing et al., 2025), SENTINEL (Peng et al., 2025), HA-DPO (Zhao et al., 2024), RLAIF-V (Yu et al., 2025), TPO (He et al., 2024), POVID (Zhou et al., 2024a), HSA-DPO (including Vanilla DPO) (Xiao et al., 2025) and mDPO (Wang et al., 2024a). All baseline results are reproduced using publicly available model weights or the provided preference datasets.

## 4.2. Main Results

In Table 1, we present a comprehensive comparison of various vision-language alignment frameworks across both hallucination-oriented and general VQA benchmarks, using LLaVA-v1.5-7B and LLaVA-v1.5-13B (Liu et al., 2023) as backbone models. Experimental results demonstrate that our method achieves state-of-the-art performance across multiple evaluation datasets. Specifically, for the LLaVA-v1.5-7B model, our method significantly reduces hallucination rates compared to the baseline, achieving a maximum reduction of up to 92%. Compared to the previous leading method SENTINEL (Peng et al., 2025), our approach yields average performance gains of 27.3% on Obj-Hal and 13.1% on AMBER. Furthermore, our method consistently achieves SOTA results on hallucination benchmarks for the 13B model, underscoring its robust generalizability on larger model scales. Regarding general VQA benchmarks, while a marginal performance trade-off is observed in certain metrics compared to the baseline, such a phenomenon is expected in hallucination mitigation approaches. As discussed in our math-

ematical explanation, the suppression of over-reliance on language priors can inherently interfere with the VLM’s internal knowledge base. Nevertheless, our approach still maintains highly competitive performance on general VQA tasks, even achieving the best results in several categories.

## 4.3. Results on MOH benchmark

**Statistics in HIIIs.** As introduced in subsection 3.3, we curate the MOH benchmark by taking the intersection of multiple model-specific HII datasets, resulting in a collection of samples that are most prone to trigger VLM hallucinations. Consequently, by conducting a statistical analysis of the MOH dataset, we can identify common hallucination patterns across VLMs with various model scales and architectures. Furthermore, we can infer the specific contexts in which VLMs are likely to falsely claim the existence of particular objects. In Figure 5, we present the top-5 objects which are most frequently hallucinated by VLMs within specific scenes, yielding several noteworthy observations. For instance, VLMs exhibit a strong tendency to hallucinate a “sink” in bathroom settings, a “boat” in waterfront scenarios, and a “train” on railroads. These findings suggest that the scene-conditioned hallucination is rooted in VLMs. For more HII examples, please refer to Appendix F.

**Evaluation on existing methods.** We evaluate prior state-of-the-art methods on our MOH benchmark and present the experimental results in Table 2 and Table 3. For baseline models, the generative task (DDG) exhibits a higher Hallucination Rate (HR) compared to the discriminative task. We hypothesize that VLMs are more prone to hallucinating when generating verbose responses due to the autoregressive nature of the models, where errors tend to accumulate over successive time steps. Among existing approaches, average hallucination rates reach as high as 47.8% and 49.4% on discriminative and generative tasks, respectively, underscoring the persistence of scene-conditioned hallucinations in current VLMs. In contrast, our method consistently reduces hallucination rates in both discriminative and generative tasks. Specifically, our approach achieves an average reduction in hallucination rates of 41.6% for the discriminative task and 73.4% for the generative task, demonstrating its effectiveness in suppressing these scene-conditioned hallucination patterns. Notably, we find that VCA-based methods (Xing et al., 2025; Wang et al., 2024a) are particularly effective at mitigating hallucinations in the discriminative task; we provide a more in-depth discussion on this observation in subsection 4.5.

## 4.4. Ablation Study

We conduct a series of ablation studies to further analyze the effectiveness of HII-DPO using LLaVA-v1.5-7B as the baseline. We present more ablation studies in Appendix D.

Table 1. Comparison with state-of-the-art methods on hallucination and general benchmarks. Best results are **bold** and second best are underlined.

Model	Method	Hallucination benchmarks						General benchmarks					Avg Rank
		Object HalBench		AMBER		HallusionBench		VQAv2		TextVQA		ScienceQA	MM-Vet
		CHAIR <sub>s.</sub> ↓	CHAIR <sub>i.</sub> ↓	CHAIR ↓	Hal. ↓	Cog. ↓	qAcc. ↑	Acc. ↑	Acc. ↑	Image Acc. ↑	Overall ↑		
LLaVA-v1.5-7B	baseline	52.7	28.0	8.4	35.5	4.0	46.86	<b>78.5</b>	<b>58.2</b>	66.8	31.0	6.50	
	Re-Align (Xing et al., 2025)	36.2	16.3	5.0	26.8	1.9	<b>47.62</b>	71.9	48.0	66.6	28.8	6.35	
	mDPO (Wang et al., 2024a)	30.7	16.0	5.0	27.5	2.4	46.15	-	47.3	67.3	-	6.18	
	HA-DPO (Zhao et al., 2024)	37.0	20.9	6.7	30.9	3.3	<b>47.74</b>	77.6	<b>56.7</b>	<b>69.7</b>	30.6	5.55	
	POVID (Zhou et al., 2024a)	33.4	16.6	5.3	28.7	3.0	46.59	77.2	56.6	68.8	31.8	5.60	
	RLAIF-V (Yu et al., 2025)	7.8	4.2	<u>2.8</u>	15.7	<u>0.9</u>	35.43	75.2	55.1	68.2	29.9	4.85	
	TPO (He et al., 2024)	5.6	3.2	3.6	20.5	1.6	40.12	75.9	55.3	67.1	25.7	5.30	
	SENTINEL (Peng et al., 2025)	<u>5.5</u>	<u>3.0</u>	2.9	<u>14.6</u>	<u>1.2</u>	47.56	<u>78.4</u>	<b>58.2</b>	<u>69.2</u>	<u>32.6</u>	<u>2.40</u>	
LLaVA-v1.5-13B	<b>HII-DPO</b>	<b>4.0</b>	<b>2.5</b>	<b>2.7</b>	<b>13.5</b>	<b>0.9</b>	<b>47.74</b>	77.8	<b>58.2</b>	68.6	<b>33.8</b>	<b>1.70</b>	

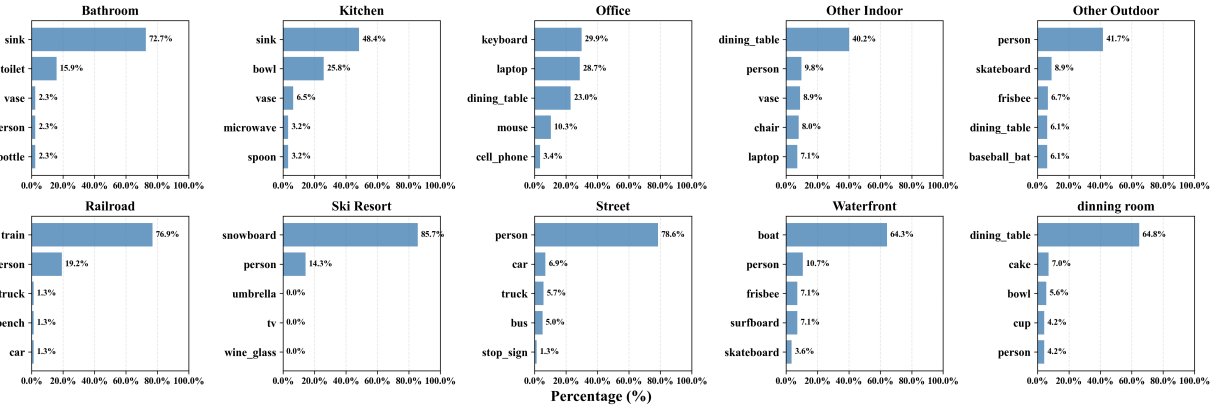


Figure 5. Distribution of the top-5 masked objects across ten environmental settings. Each subplot illustrates the percentage of specific objects that trigger hallucinations within the scenario. These statistics reveal the ingrained scene-conditioned hallucination pattern within VLMs; for instance, “boat” dominates in waterfront context, while “train” is the primary driver of hallucinations in the railroad setting.

Table 2. Results on the MOH benchmark for LLaVA-v1.5-7B. We report the hallucination rates  $HR^D$  and  $HR^G$

Metric	Baseline	Re-Align	mDPO	POVID	HA-DPO	TPO	SENTINEL	Ours
$HR^D \downarrow$	52.2	49.9	50.7	51.1	45.2	31.7	38.3	<b>28.1</b>
$HR^G \downarrow$	68.6	49.0	53.2	65.1	63.4	36.6	38.8	<b>18.8</b>

Table 3. Results on the MOH benchmark for LLaVA-v1.5-13B.

Metric	Baseline	Re-Align	mDPO	vanilla-DPO	HSA-DPO	SENTINEL	Ours
$HR^D \downarrow$	69.5	<b>39.4</b>	45.6	46.2	45.3	56.8	43.8
$HR^G \downarrow$	67.9	51.1	48.3	35.0	28.2	36.5	<b>17.5</b>

**Mask threshold.** In this part, we evaluate the impact of the confidence threshold within the HII Synthesis Pipeline in Figure 2 and summarize the empirical results in Table 5. We observe that a lower threshold often leads to the inaccurate detection of entity labels, introducing semantic ambiguity and noise into the preference pairs, which can ultimately exacerbate hallucinations. Conversely, an excessively high threshold may filter out valid labels and restrict the yield of HII, thereby diminishing the diversity of the training data.

Overall, 0.35 is the optimal choice for balancing detection robustness with the preservation of sample diversity.

**Iterative masking strategy.** We further evaluate the effectiveness of the iterative masking strategy within the HII Synthesis Pipeline (Figure 2). As illustrated by the experimental results in Table 6, the iterative approach consistently outperforms the single-pass masking baseline. Relying solely on an initial mask often leads to incomplete occlusion of the target entity. Consequently, the open-vocabulary detector may still identify remnants of the partially masked object during dataset generation, thereby introducing semantic ambiguity into the resulting preference pairs.

#### 4.5. Comparison with VCA-based Methods

As previously discussed, mDPO (Wang et al., 2024a) pioneered the integration of Vision-Contrastive Alignment (VCA) datasets into the DPO framework. This approach can be formally defined as:

**Table 4. Comparison with existing VCA-based methods on hallucination and general benchmarks.** We evaluate the integration of our HIIIs with the SENTINEL framework. While the results show that SENTINEL + HIIIs achieves a new state-of-the-art in hallucination suppression, it incurs an inevitable performance degradation in general understanding capabilities.

Model	Method	Hallucination benchmarks						General benchmarks				
		Object HalBench		AMBER			MOH		VQAv2	TextVQA	ScienceQA	MM-Vet
		CHAIR.s. ↓	CHAIR.i. ↓	CHAIR ↓	Hal. ↓	Cog. ↓	HR <sup>D</sup> . ↓	HR <sup>G</sup> . ↓	Acc. ↑	Acc. ↑	Image Acc. ↑	Overall ↑
LLaVA-v1.5-7B	baseline	52.7	28.0	8.4	35.5	4.0	52.2	68.6	<b>78.5</b>	<b>58.2</b>	66.8	31.0
	Re-Align	36.2	16.3	5.0	26.8	1.9	49.9	49.0	71.9	48.0	66.6	28.8
	mDPO	30.7	16.0	5.0	27.5	2.4	50.7	53.2	-	47.3	67.3	-
	SENTINEL	5.5	3.0	2.9	14.6	1.2	38.3	38.8	78.4	<b>58.2</b>	<b>69.2</b>	<b>32.6</b>
	SENTINEL + HIIIs	1.5	1.0	1.6	6.7	0.4	13.5	8.6	77.0	57.5	67.9	32.2

**Table 5. Ablation study on the detection threshold in the entity detection phase.**

Threshold	Object HalBench		AMBER			ScienceQA
	CHAIR.s. ↓	CHAIR.i. ↓	CHAIR ↓	Hal ↓	Cog ↓	Image Acc. ↑
Baseline	52.7	27.9	8.4	35.5	4.0	66.8
0.25	7.2	3.0	3.2	14.6	1.2	67.9
0.35	<b>4.0</b>	<b>2.5</b>	<b>2.7</b>	<b>13.5</b>	<b>0.9</b>	<b>68.6</b>
0.45	9.3	3.2	3.0	15.4	1.2	67.5

**Table 6. Ablation study on the iterative masking strategy.**

Method	Object HalBench		AMBER			ScienceQA
	CHAIR.s. ↓	CHAIR.i. ↓	CHAIR ↓	Hal ↓	Cog ↓	Image Acc. ↑
LLaVA-v1.5-7B	52.7	27.9	8.4	35.5	4.0	66.8
w.o. iterative	9.2	3.6	3.6	15.6	1.2	67.2
w. iterative	<b>4.0</b>	<b>2.5</b>	<b>2.7</b>	<b>13.5</b>	<b>0.9</b>	<b>68.6</b>

Here,  $v^+$  denotes the original natural image, while  $v^-$  represents a visually corrupted or irrelevant image.  $y^+$  is the chosen response paired with  $v^+$ . As shown in [Table 2](#) and [Table 3](#), VCA-based methods effectively reduce hallucination rates on the MOH benchmark. Motivated by these findings, we leverage HIIIs as the negative vision-contrastive signals ( $v^-$ ) and the corresponding unmasked natural images as the positive signals ( $v^+$ ) to investigate the efficacy of HIIIs within the VCA paradigm. Specifically, we augmented the original training dataset provided by SENTINEL ([Peng et al., 2025](#)) with our HII samples and conducted extensive evaluations. As shown in [Table 4](#), incorporating HIIIs as vision-contrastive signals drastically mitigates hallucination rates across all evaluated benchmarks, including MOH. However, this reduction comes at the expense of general understanding capabilities—a trade-off we further analyze in the following part. As previously discussed in [Section 1](#), DPO inherently decreases the probability of the chosen response  $y^+$  when paired with the negative image  $v^-$ , even if portions of  $y^+$  contain semantic details that remain

grounded in  $v^-$ . This leads to two primary consequences: **(1) Conservative Model Behavior:** Since the DPO objective suppresses the likelihood of  $y^+$  when paired with the negative image  $v^-$ , even the semantic elements that remain factually grounded in  $v^-$  are inevitably penalized. This often leads to an *over-correction* effect, where the VLM adopts a more conservative generation strategy. Consequently, the model exhibits an increased tendency toward brevity, becoming more reluctant to provide detailed descriptions or venture into fine-grained inferences for ambiguous visual regions to minimize the risk of penalty. **(2) Erosion of the Internal Knowledge Base:** While the Vision-Contrastive Alignment (VCA) paradigm effectively disrupts harmful linguistic biases, it may simultaneously erode the model’s internal knowledge base acquired during the Supervised Fine-Tuning (SFT) phase. This is primarily attributed to the unconditional penalization of the chosen response  $y^+$  when paired with the negative image  $v^-$ . The resulting suppression of these established priors leads to a degradation in performance on general VQA tasks, where the model previously relied on such internal knowledge to bridge visual gaps.

## 5. Conclusion

Driven by the scene-object co-occurrence, we propose a systematic framework to investigate and mitigate the scene-conditioned hallucination pattern. We design a pipeline to synthesize model-specific Hallucination-Induced Images and subsequently extract their intersection to uncover universal hallucination patterns shared across various model architectures and scales. Based on HIIIs, we introduce the MOH benchmark to rigorously evaluate a VLM’s susceptibility to language bias. Furthermore, we leverage HIIIs to construct preference datasets and employ HII-DPO to perform fine-grained preference alignment. Our experimental results demonstrate that this approach significantly mitigates hallucinations while preserving the general capabilities of the models.

## Impact Statement

Our work proposes HII-DPO a novel framework to mitigate scene-conditioned hallucinations in Vision-Language Models (VLMs). By prioritizing visual grounding over linguistic shortcuts, our method significantly enhances the reliability of AI. This is particularly critical in domains such as medical diagnostics and autonomous navigation, where factual accuracy and robust verification are indispensable for operational safety. Furthermore, our approach helps identify and suppress ingrained language biases, promoting more objective multimodal reasoning. Additionally, the proposed HII pipeline serves as a robust diagnostic instrument for the research community to systematically investigate and address model vulnerabilities.

## References

Achiam, J., Adler, S., Agarwal, S., Ahmad, L., Akkaya, I., Aleman, F. L., Almeida, D., Altenschmidt, J., Altman, S., Anadkat, S., et al. Gpt-4 technical report. *arXiv preprint arXiv:2303.08774*, 2023.

Bai, J., Bai, S., Yang, S., Wang, S., Tan, S., Wang, P., Lin, J., Zhou, C., and Zhou, J. Qwen-vl: A versatile vision-language model for understanding, localization, text reading, and beyond, 2023. URL <https://arxiv.org/abs/2308.12966>.

Bai, S., Chen, K., Liu, X., Wang, J., Ge, W., Song, S., Dang, K., Wang, P., Wang, S., Tang, J., Zhong, H., Zhu, Y., Yang, M., Li, Z., Wan, J., Wang, P., Ding, W., Fu, Z., Xu, Y., Ye, J., Zhang, X., Xie, T., Cheng, Z., Zhang, H., Yang, Z., Xu, H., and Lin, J. Qwen2.5-vl technical report, 2025. URL <https://arxiv.org/abs/2502.13923>.

Bradley, R. A. and Terry, M. E. Rank analysis of incomplete block designs: I. the method of paired comparisons. *Biometrika*, 39(3/4):324–345, 1952.

Chen, C., Liu, M., Jing, C., Zhou, Y., Rao, F., Chen, H., Zhang, B., and Shen, C. Perturbollava: Reducing multimodal hallucinations with perturbative visual training, 2025. URL <https://arxiv.org/abs/2503.06486>.

Chiang, W.-L., Li, Z., Lin, Z., Sheng, Y., Wu, Z., Zhuang, S., Li, Y., Li, H., Zhang, E., Skowron, A., et al. Vicuna: An open-source chatbot impressing gpt-4 with 90% chatgpt quality. *arXiv preprint arXiv:2303.13512*, 2023.

Dosovitskiy, A., Beyer, L., Kolesnikov, A., Weissenborn, D., Zhai, X., Unterthiner, T., Dehghani, M., Minderer, M., Heigold, G., Gelly, S., Uszkoreit, J., and Houlsby, N. An image is worth 16x16 words: Transformers for image recognition at scale. In *International Conference on Learning Representations (ICLR)*, 2021.

Goyal, Y., Khot, T., Summers-Stay, D., Batra, D., and Parikh, D. Making the v in vqa matter: Elevating the role of image understanding in visual question answering. In *Proceedings of the IEEE Conference on Computer Vision and Pattern Recognition (CVPR)*, July 2017a.

Goyal, Y., Khot, T., Summers-Stay, D., Batra, D., and Parikh, D. Making the v in vqa matter: Elevating the role of image understanding in visual question answering. In *Proceedings of the IEEE conference on computer vision and pattern recognition*, pp. 6904–6913, 2017b.

Gu, Y., Zhang, W., Lyu, C., Lin, D., and Chen, K. Mask-dpo: Generalizable fine-grained factuality alignment of llms, 2025. URL <https://arxiv.org/abs/2503.02846>.

Guan, T., Liu, F., Wu, X., Xian, R., Li, Z., Liu, X., Wang, X., Chen, L., Huang, F., Yacoob, Y., et al. Hallusionbench: an advanced diagnostic suite for entangled language hallucination and visual illusion in large vision-language models. In *Proceedings of the IEEE/CVF Conference on Computer Vision and Pattern Recognition*, pp. 14375–14385, 2024.

He, L., Chen, Z., Shi, Z., Yu, T., Shao, J., and Sheng, L. A topic-level self-correctional approach to mitigate hallucinations in mllms. *arXiv preprint arXiv:2411.17265*, 2024.

Krishna, R., Zhu, Y., Groth, O., Johnson, J., Hata, K., Kravitz, J., Chen, S., Kalantidis, Y., Li, L.-J., Shamma, D. A., et al. Visual genome: Connecting language and vision using crowdsourced dense image annotations. *International journal of computer vision*, 123(1):32–73, 2017.

Li, H., Zhu, J., Chen, Y., et al. Hsa-dpo: Human-style alignment for large vision-language models via hierarchical self-alignment. *arXiv preprint arXiv:2406.01797*, 2024.

Lin, T.-Y., Maire, M., Belongie, S., Bourdev, L., Girshick, R., Hays, J., Perona, P., Ramanan, D., Zitnick, C. L., and Dollár, P. Microsoft coco: Common objects in context, 2015. URL <https://arxiv.org/abs/1405.0312>.

Liu, H., Li, C., Wu, Q., and Lee, Y. J. Visual instruction tuning, 2023. URL <https://arxiv.org/abs/2304.08485>.

Liu, S., Zeng, Z., Ren, T., Li, F., Zhang, H., Yang, J., Jiang, Q., Li, C., Yang, J., Su, H., et al. Grounding dino: Marrying dino with grounded pre-training for open-set object detection. In *European conference on computer vision*, pp. 38–55. Springer, 2024.

Lu, J., Yang, J., Batra, D., and Parikh, D. Neural baby talk. In *Proceedings of the IEEE Conference on Computer Vision and Pattern Recognition (CVPR)*, June 2018.

Lu, P., Mishra, S., Xia, T., Qiu, L., Chang, K.-W., Zhu, S.-C., Tafjord, O., Clark, P., and Kalyan, A. Learn to explain: Multimodal reasoning via thought chains for science question answering. *Advances in Neural Information Processing Systems*, 35:2507–2521, 2022.

Peng, S., Yang, S., Jiang, L., and Tian, Z. Mitigating object hallucinations via sentence-level early intervention, 2025. URL <https://arxiv.org/abs/2507.12455>.

Radford, A., Kim, J. W., Hallacy, C., Ramesh, A., Goh, G., Agarwal, S., Sastry, G., Askell, A., Mishkin, P., Clark, J., Krueger, G., and Sutskever, I. Learning transferable visual models from natural language supervision. In *Proceedings of the International Conference on Machine Learning (ICML)*, 2021.

Rafailov, R., Sharma, A., Mitchell, E., and Finn, C. Direct preference optimization: Your language model is secretly a reward model. *arXiv preprint arXiv:2305.18290*, 2023.

Rafailov, R., Sharma, A., Mitchell, E., Ermon, S., Manning, C. D., and Finn, C. Direct preference optimization: Your language model is secretly a reward model, 2024. URL <https://arxiv.org/abs/2305.18290>.

Rajbhandari, S., Rasley, J., Ruwase, O., and He, Y. Zero: Memory optimizations toward training trillion parameter models. In *SC20: International Conference for High Performance Computing, Networking, Storage and Analysis*, pp. 1–16. IEEE, 2020.

Rohrbach, A., Hendricks, L. A., Burns, K., Darrell, T., and Saenko, K. Object hallucination in image captioning. In *Proceedings of the 2018 Conference on Empirical Methods in Natural Language Processing (EMNLP)*, 2018.

Singh, A., Natarajan, V., Shah, M., Jiang, Y., Chen, X., Batra, D., Parikh, D., and Rohrbach, M. Towards vqa models that can read. In *Proceedings of the IEEE/CVF Conference on Computer Vision and Pattern Recognition (CVPR)*, June 2019a.

Singh, A., Natarajan, V., Shah, M., Jiang, Y., Chen, X., Batra, D., Parikh, D., and Rohrbach, M. Towards vqa models that can read. In *Proceedings of the IEEE/CVF conference on computer vision and pattern recognition*, pp. 8317–8326, 2019b.

Touvron, H., Lavril, T., Izacard, G., Martinet, X., Lachaux, M.-A., Lacroix, T., Rozière, B., Goyal, N., Hambro, E., Azhar, F., Rodriguez, A., Joulin, A., Grave, E., and Lample, G. Llama: Open and efficient foundation language models. *arXiv preprint arXiv:2302.13971*, 2023.

Wang, F., Zhou, W., Huang, J. Y., Xu, N., Zhang, S., Poon, H., and Chen, M. mdpo: Conditional preference optimization for multimodal large language models, 2024a. URL <https://arxiv.org/abs/2406.11839>.

Wang, J., Wang, Y., Xu, G., Zhang, J., Gu, Y., Jia, H., Wang, J., Xu, H., Yan, M., Zhang, J., and Sang, J. Amber: An llm-free multi-dimensional benchmark for mllms hallucination evaluation, 2024b. URL <https://arxiv.org/abs/2311.07397>.

Wang, P., Bai, S., Tan, S., Wang, S., Fan, Z., Bai, J., Chen, K., Liu, X., Wang, J., Ge, W., Fan, Y., Dang, K., Du, M., Ren, X., Men, R., Liu, D., Zhou, C., Zhou, J., and Lin, J. Qwen2-vl: Enhancing vision-language model’s perception of the world at any resolution, 2024c. URL <https://arxiv.org/abs/2409.12191>.

Xiao, W., Huang, Z., Gan, L., He, W., Li, H., Yu, Z., Shu, F., Jiang, H., and Zhu, L. Detecting and mitigating hallucination in large vision language models via fine-grained ai feedback, 2025. URL <https://arxiv.org/abs/2404.14233>.

Xing, S., Li, P., Wang, Y., Bai, R., Wang, Y., Hu, C.-W., Qian, C., Yao, H., and Tu, Z. Re-align: Aligning vision language models via retrieval-augmented direct preference optimization, 2025. URL <https://arxiv.org/abs/2502.13146>.

Xiong, Y., Yang, H., and Li, Y. A survey on hallucination in large vision-language models. *arXiv preprint arXiv:2402.00253*, 2024. URL <https://arxiv.org/abs/2402.00253>.

Yang, A., Bai, J., Zhang, M., and et al. Qwen2 technical report. *arXiv preprint arXiv:2407.10671*, 2024.

Yu, T., Zhang, H., Li, Q., Xu, Q., Yao, Y., Chen, D., Lu, X., Cui, G., Dang, Y., He, T., et al. Rlaif-v: Open-source ai feedback leads to super gpt-4v trustworthiness. In *Proceedings of the Computer Vision and Pattern Recognition Conference*, pp. 19985–19995, 2025.

Yu, W., Yang, Z., Li, L., Wang, J., Lin, K., Liu, Z., Wang, X., and Wang, L. Mm-vet: Evaluating large multimodal models for integrated capabilities. *arXiv preprint arXiv:2308.02490*, 2023.

Zadeh, F. P., Oh, Y., and Kim, G. Lpoi: Listwise preference optimization for vision language models, 2025. URL <https://arxiv.org/abs/2505.21061>.

Zhai, X., Mustafa, B., Kolesnikov, A., and Beyer, L. Siglip: Scaling vision-language models with sign language pre-training. In *Proceedings of the IEEE/CVF International Conference on Computer Vision (ICCV)*, 2023.

Zhang, Y.-F., Yu, T., Tian, H., Fu, C., Li, P., Zeng, J., Xie, W., Shi, Y., Zhang, H., Wu, J., Wang, X., Hu, Y., Wen, B., Yang, F., Zhang, Z., Gao, T., Zhang, D., Wang, L., Jin, R., and Tan, T. Mm-rlhf: The next step forward in multimodal llm alignment, 2025. URL <https://arxiv.org/abs/2502.10391>.

Zhao, H., Li, Y., Ma, X., et al. Evaluating object hallucination in large vision-language models. *arXiv preprint arXiv:2305.10355*, 2023.

Zhao, Z., Wang, B., Ouyang, L., Dong, X., Wang, J., and He, C. Beyond hallucinations: Enhancing lylms through hallucination-aware direct preference optimization, 2024. URL <https://arxiv.org/abs/2311.16839>.

Zhou, Y., Cui, C., Rafailov, R., Finn, C., and Yao, H. Aligning modalities in vision large language models via preference fine-tuning, 2024a. URL <https://arxiv.org/abs/2402.11411>.

Zhou, Y., Cui, C., Yoon, J., Zhang, L., Deng, Z., Finn, C., Bansal, M., and Yao, H. Analyzing and mitigating object hallucination in large vision-language models, 2024b. URL <https://arxiv.org/abs/2310.00754>.

## A. Mathematical Explanation

We provide a probabilistic view of why *HII*s are effective for preference alignment in mitigating object hallucination. For a given object  $o$ , define:

- $v$ : the original image (where  $o$  is truly present).
- $v' = v - o$ : a hallucination-inducing image where  $o$  is removed (or masked out).
- $x$ : the textual context providing an accurate but partial description of the input image.
- $z \in \{0, 1\}$ : a binary variable indicating whether the model *claims* that  $o$  is present in the image ( $z = 1$ ) or absent ( $z = 0$ ).
- $p_\theta(\cdot)$ : the VLM parameterized by  $\theta$ .

We focus on the model's propensity to assert the presence of  $o$  given  $(x, v)$ :

$$p_\theta(z = 1 | x, v). \quad (8)$$

By Bayes' rule,

$$\begin{aligned} p_\theta(z = 1 | x, v) &= \frac{p_\theta(v | z = 1, x) p_\theta(z = 1 | x)}{p_\theta(v | x)} \\ &\propto p_\theta(v | z = 1, x) p_\theta(z = 1 | x), \end{aligned} \quad (9)$$

where  $p_\theta(v | x)$  is the normalization term for *fixed*  $(x, v)$ . In this formulation,  $p_\theta(z = 1 | x)$  captures the *language prior*, representing the model's inherent expectation of object  $o$  given the textual context  $x$ . And  $p_\theta(v | z = 1, x)$  is interpreted as the *visual likelihood*, which quantifies the compatibility between the observed visual evidence and the hypothesis of  $o$ 's presence. Although standard VLMs do not explicitly parameterize these components, they are implicitly optimized during our preference alignment process to achieve a better balance between textual priors and visual evidence.

A more revealing form is obtained by considering *posterior odds*. Using the identity

$$\frac{p_\theta(z = 1 | x, v)}{p_\theta(z = 0 | x, v)} = \frac{p_\theta(v | z = 1, x)}{p_\theta(v | z = 0, x)} \cdot \frac{p_\theta(z = 1 | x)}{p_\theta(z = 0 | x)},$$

we get the log-odds decomposition:

$$\begin{aligned} \log \frac{p_\theta(z = 1 | x, v)}{p_\theta(z = 0 | x, v)} &= \underbrace{\log \frac{p_\theta(v | z = 1, x)}{p_\theta(v | z = 0, x)}}_{\text{visual evidence (likelihood ratio)}} \\ &+ \underbrace{\log \frac{p_\theta(z = 1 | x)}{p_\theta(z = 0 | x)}}_{\text{language prior (prior odds)}}. \end{aligned} \quad (10)$$

**Why hallucinations happen after SFT.** In many caption/instruction-tuning corpora, objects co-occur in stereotypical ways. As a result, after SFT the prior odds can become highly skewed, i.e.,  $p_\theta(z = 1 | x) \gg p_\theta(z = 0 | x)$  for certain objects, even when the image does not support them. Then the second term in Equation 10 can dominate, pushing the model to claim  $z = 1$  (hallucination) despite weak or contradictory visual evidence.

**Why HII<sub>s</sub> help.** Now consider the edited image  $v' = v - o$ , where  $o$  is absent. The desired behavior is to increase

$$p_\theta(z = 0 | x, v') \propto p_\theta(v' | z = 0, x) p_\theta(z = 0 | x). \quad (11)$$

Crucially,  $v'$  often preserves the contextual cues that correlate with  $o$  (scene, co-occurring objects, typical layouts), so the language prior may still favor  $z = 1$ . Thus,  $v'$  creates hard counterexamples where the model must rely on visual grounding (negative evidence) instead of the scene-object co-occurrence heuristics.

In preference alignment, we provide pairs consisting of: (i) a *chosen* response  $y^+$  that correctly omits any mention of object  $o$ , and (ii) a *rejected* response  $y^-$  that falsely claims the existence of  $o$  for the same  $(x, v')$ . Optimizing the preference objective increases the model’s probability of producing  $y^+$  over  $y^-$ , which effectively increases the posterior odds:  $p_\theta(z = 0 | x, v')$ . Viewed through Equation 10, this can be achieved in two complementary ways:

- **Strengthening visual grounding:** increasing the likelihood ratio in favor of absence, i.e., making  $p_\theta(v' | z = 0, x)$  relatively larger than  $p_\theta(v' | z = 1, x)$  by learning features that recognize missing objects / masked regions.
- **Weakening language priors:** reducing the prior odds  $\frac{p_\theta(z=1|x)}{p_\theta(z=0|x)}$ , i.e., learning that certain objects are *not necessary* given  $x$  and the remaining scene context.

Therefore, HII directly target the failure mode where language priors overwhelm visual evidence, by repeatedly presenting situations where the prior expectation is wrong but the visual signal is clear.

**Trade-off.** Reducing overly strong language priors can sometimes lower performance when the prompt is under-specified and the model must rely on commonsense completion. We discuss this capability–hallucination trade-off in section 4.

## B. Experiments on Qwen-Family

Table 7. Experimental results on the Qwen-family models.

Model	Method	Hallucination benchmarks				General benchmarks		
		Object HalBench		MOH		TextVQA	ScienceQA	MM-Vet
		CHAIR-s. ↓	CHAIR-i. ↓	HR <sup>D</sup> . ↓	HR <sup>G</sup> . ↓	Acc. ↑	Image Acc. ↑	Overall ↑
Qwen2-VL-2B-Instruct	baseline	15.3	8.6	4.1	59.0	78.3	76.9	49.4
	<b>Ours</b>	2.9 <b>+12.4</b>	1.7 <b>+6.9</b>	4.7 <b>-0.6</b>	15.5 <b>+43.5</b>	78.2 <b>-0.1</b>	76.9 <b>+0.0</b>	50.3 <b>+0.9</b>
Qwen2-VL-7B-Instruct	baseline	14.3	8.5	11.5	58.0	82.2	85.7	62.7
	<b>Ours</b>	4.2 <b>+10.1</b>	2.5 <b>+6.0</b>	9.0 <b>+2.5</b>	20.0 <b>+38.0</b>	82.3 <b>+0.1</b>	86.7 <b>+1.0</b>	62.7 <b>+0.0</b>
Qwen2.5-VL-7B-Instruct	baseline	15.0	9.2	3.6	47.0	77.7	88.6	72.0
	<b>Ours</b>	2.8 <b>+13.2</b>	1.6 <b>+7.6</b>	2.2 <b>+1.4</b>	17.4 <b>+29.6</b>	78.4 <b>+0.7</b>	88.5 <b>-0.1</b>	69.8 <b>-2.2</b>

To demonstrate the architectural robustness of our approach, we extend our evaluation to the latest Qwen2-VL and Qwen2.5-VL series. As shown in Table 7, the empirical results indicate that our method consistently mitigates hallucinations across both standard benchmarks and the specialized MOH benchmark. While certain metrics on general capability benchmarks exhibit marginal degradation, the overall performance remains highly competitive. This confirms that HII-DPO successfully suppresses scene-conditioned hallucinations without compromising the model’s general understanding capability.

## C. Examples of the Synonym Dictionary for Entity Normalization.

We built the synonym dictionary based on the list from (Lu et al., 2018; Rohrbach et al., 2018). Here are some examples of the synonym dictionary:

<b>Person</b>	{girl, boy, man, woman, kid, child, chef, baker, people, rider, children, worker, sister, brother, ...}
<b>Bird</b>	{ostrich, owl, seagull, goose, duck, parakeet, falcon, robin, pelican, waterfowl, heron, ...}
<b>Dog</b>	{puppy, beagle, pup, chihuahua, schnauzer, dachshund, rottweiler, canine, pitbull, collie, ...}
<b>Horse</b>	{colt, pony, racehorse, stallion, equine, mare, foal, palomino, mustang, clydesdale, bronco, ...}
<b>Cow</b>	{cattle, oxen, ox, calf, holstein, heifer, buffalo, bull, zebu, bison}
<b>Boat</b>	{ship, liner, sailboat, motorboat, dinghy, powerboat, speedboat, canoe, skiff, yacht, kayak, vessel, ...}
<b>Car</b>	{automobile, van, minivan, sedan, suv, hatchback, cab, jeep, coupe, taxicab, limo, taxi}
<b>Airplane</b>	{jetliner, plane, air plane, monoplane, aircraft, jet, airbus, biplane, seaplane}
<b>Train</b>	{locomotive, tramway, caboose}

<b>Traffic Light</b>	{street light, traffic signal, stop light, streetlight, stoplight}
<b>Sandwich</b>	{burger, sub, cheeseburger, hamburger}
<b>Cake</b>	{cheesecake, cupcake, shortcake, coffeecake, pancake}
<b>Couch</b>	{sofa, recliner, futon, loveseat, settee, chesterfield}
<b>Laptop</b>	{computer, notebook, netbook, lenovo, macbook, laptop computer}
<b>Phone</b>	{cell phone, mobile phone, cellphone, telephone, phon, smartphone, iPhone}

## D. More Ablation Studies

Table 8. Ablation study on the response generation strategy.

Method	Object HalBench		AMBER			ScienceQA
	CHAIR_s. ↓	CHAIR_i. ↓	CHAIR ↓	Hal ↓	Cog ↓	Image Acc. ↑
Baseline	52.7	27.9	8.4	35.5	4.0	66.8
whole response	12.5	4.6	3.6	16.9	1.6	67.5
sentence-by-sentence	<b>4.0</b>	<b>2.5</b>	<b>2.7</b>	<b>13.5</b>	<b>0.9</b>	<b>68.6</b>

**Sentence-by-sentence strategy.** We also investigate the effectiveness of the sentence-by-sentence strategy in dataset generation. As detailed in Table 8, we conduct a comparative analysis between the whole-response and sentence-by-sentence strategies. The results suggest that the latter achieves superior performance across both hallucination benchmarks and general VQA tasks. We hypothesize that this improvement stems from two primary factors **(1) Granularity of Reward Signals:** The whole-response strategy often yields rejected responses that conflate factual and hallucinated information simultaneously (Gu et al., 2025), which can lead to corrupted reward signals during preference alignment. Conversely, the sentence-by-sentence strategy constructs preference pairs at the individual sentence level, ensuring fine-grained and more precise optimization signals. **(2) Enhanced Data Diversity:** While the whole-response strategy typically generates only a single preference pair per image, the sentence-by-sentence approach enables the extraction of multiple preference pairs from a single image-response interaction, significantly increasing the diversity of the training data.

Table 9. Ablation study on different prompt types ( $N$ ).

N	Object HalBench		AMBER			ScienceQA	MM-Vet
	CHAIR_s. ↓	CHAIR_i. ↓	CHAIR ↓	Hal ↓	Cog ↓	Image Acc. ↑	Overall ↑
Baseline	52.7	27.9	8.4	35.5	4.0	66.8	31.0
2	7.2	4.0	3.2	14.5	1.2	67.9	32.9
3	4.0	2.5	2.7	13.5	<b>0.9</b>	<b>68.6</b>	<b>33.8</b>
4	<b>2.9</b>	<b>2.3</b>	<b>2.5</b>	<b>11.9</b>	<b>0.9</b>	67.5	33.2

**Prompts in dataset generation.** To ensure diversity in dataset generation, we utilize multiple instructions for each HII when generating preference datasets. Specifically, we randomly select  $N$  prompts from the following collection:

- “What is this photo about? Please answer in great detail.”
- “Describe this image in detail.”
- “Provide a thorough description of the given picture.”
- “Please provide a detailed description of the picture.”
- “Take a look at this image and describe what you notice.”
- “Could you describe the contents of this image for me?”

Table 10. Ablation study on model-specific HII filtering.

Method	Hallucination benchmarks							General benchmarks			
	Object HalBench		AMBER			MOH		VQAv2	TextVQA	ScienceQA	MM-Vet
	CHAIR.s. ↓	CHAIR.i. ↓	CHAIR ↓	Hal. ↓	Cog. ↓	HR <sup>D</sup> . ↓	HR <sup>G</sup> . ↓	Acc. ↑	Acc. ↑	Image Acc. ↑	Overall ↑
baseline	52.7	28.0	8.4	35.5	4.0	52.2	68.6	<b>78.5</b>	<b>58.2</b>	66.8	31.0
random masking	9.3	3.6	3.2	15.8	1.6	40.3	37.2	78.0	<b>58.2</b>	68.4	32.8
model-specific HII	<b>4.0</b>	<b>2.5</b>	<b>2.7</b>	<b>13.5</b>	<b>0.9</b>	<b>28.1</b>	<b>18.8</b>	77.8	<b>58.2</b>	<b>68.6</b>	<b>33.8</b>

We vary the value of  $N$  and present the corresponding experimental results in Table 9. We observe that using only one prompt per HII results in suboptimal alignment due to a lack of diversity. Conversely, although a larger  $N$  (i.e.,  $N > 3$ ) further reduces hallucinations, it tends to cause overfitting, which undermines the model’s underlying knowledge and general VQA performance. Overall,  $N = 3$  strikes the ideal balance, effectively mitigating hallucinations while maintaining robust general-purpose understanding.

**Random masking vs. model-specific HII.** We additionally perform an ablation by replacing model-specific HII filtering with random object masking, while keeping all other components identical (the same detector, masking procedure, and preference-pair construction). Table 10 shows that random masking already alleviates hallucination, suggesting that high-quality counterfactual preference pairs (facilitated by GroundingDINO for accurate object localization and consistent grounding) provide a generally useful alignment signal. Nevertheless, random masks are not semantically tied to the underlying scenarios. Thus, the removed objects often do not correspond to the objects that the model would hallucinate due to strong scene-object co-occurrence priors. As a result, the preference pairs are less informative for correcting the model’s dominant failure mode (scene-conditioned hallucination), leading to weaker improvements than our model-specific HII filtering, which explicitly focuses on the scene-conditioned hallucination pattern.

## E. Training Details

### E.1. Dataset

**MSCOCO.** MSCOCO (Lin et al., 2015) is a large-scale object detection, segmentation, and captioning dataset. It comprises over 328,000 images, covering 80 object categories with more than 2.5 million labeled instances. For vision-language tasks, each image is paired with at least five human-written captions, ensuring a standard benchmark for evaluating image captioning and cross-modal retrieval models.

**Visual Genome.** Visual Genome (Krishna et al., 2017) is a densely annotated visual dataset that focuses on detailed scene semantics beyond object presence. It provides fine-grained annotations including objects, attributes, relationships, region descriptions, and scene graphs for each image. Compared to MSCOCO (Lin et al., 2015), Visual Genome offers a more exhaustive coverage of object categories and relational structures, enabling more precise analysis of object interactions and compositional semantics. These characteristics make Visual Genome particularly valuable for studying scene-conditioned hallucination patterns and for synthesizing challenging counterfactual or hallucination-inducing samples where subtle visual cues and relational dependencies are critical.

Table 11. Training hyperparameters for LLaVA-v1.5 models. Note: Weight decay is 0. Memory optimization uses Zero-2 (Rajbhandari et al., 2020).

Base Model	lr	LoRA $r$	LoRA $\alpha$	LoRA $\beta$	Proj. LR	Scheduler	Optim	Length	Epochs	Global Batch
LLaVA-v1.5-7B	2e-6	128	256	0.1	0	Cosine	AdamW	2048	1	64
LLaVA-v1.5-13B	3e-6	128	256	0.1	0	Cosine	AdamW	2048	1	64

### E.2. Training Setup

In order to ensure a fair comparison with existing methods (Peng et al., 2025; Xing et al., 2025; Xiao et al., 2025; Wang et al., 2024a; He et al., 2024; Zhao et al., 2024; Zhou et al., 2024a; Yu et al., 2025), we employ LLaVA-v1.5-7B and LLaVA-v1.5-13B (Liu et al., 2023) as our backbone models. We conduct preference alignment using the proposed HII-DPO framework. For the training configuration, we utilize LoRA fine-tuning with a rank of  $r = 128$  and an alpha of  $\alpha = 256$ .

Both the 7B and 13B models are fine-tuned for 1 epoch, with learning rates set to  $2 \times 10^{-6}$  and  $3 \times 10^{-6}$ , respectively. More details about hyperparameters are presented in [Table 11](#).

## F. HII examples

In this section, we present more HII examples to illustrate the scene-conditioned hallucination patterns in VLMs. Following our HII synthesis pipeline ([Figure 2](#)), we generate model-specific HII sets using VLMs of different scales and architectures. We then take the intersection of these model-specific HII sets to obtain the hardest counterfactual images—those that consistently trigger the same hallucinated object across models—and use them to construct MOH for rigorous evaluation of scene-conditioned hallucinations. Finally, we provide qualitative examples in [Figure 6](#) and [Figure 7](#), which highlight how scene context induces systematic object hallucinations despite the absence of visual evidence.



*Figure 6.* HII examples in **Office**, **Bathroom**, **Dining Room** and **Street** scenarios.

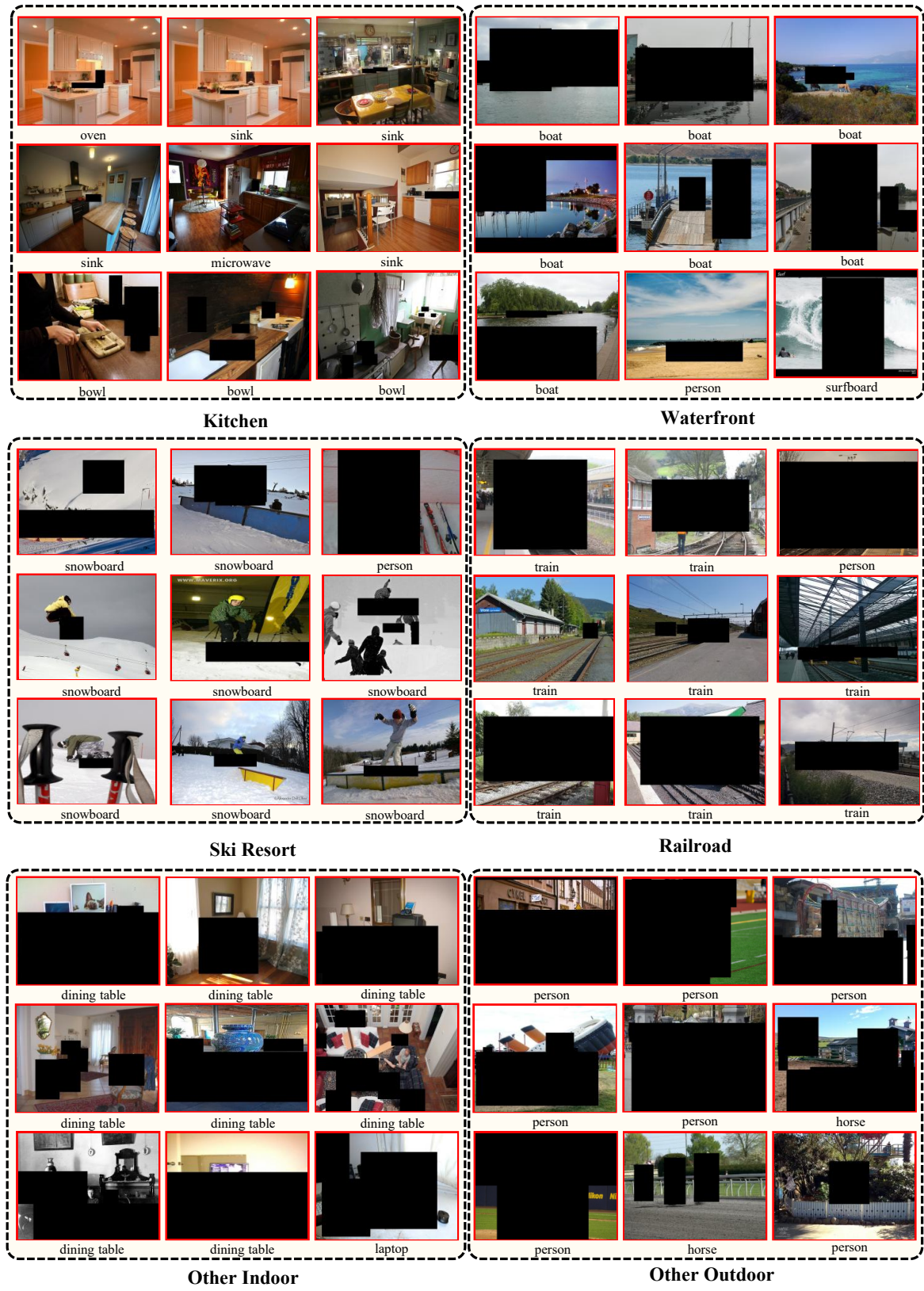


Figure 7. HII examples in **Kitchen**, **Waterfront**, **Ski Resort**, **Railroad**, **Other Indoor** and **Other Outdoor** scenarios.

## G. Additional Case Studies

To further substantiate the efficacy of our approach in mitigating the scene-conditioned hallucination pattern, we provide additional qualitative examples in [Figure 8](#) and [Figure 9](#). We compare the responses generated by the base model LLaVA-v1.5 and HII-DPO for the same HII. Given a Hallucination-Inducing Image (HII) where the specific object is removed, the base model repeatedly hallucinates the masked object and related items due to rooted scene-object co-occurrence hallucination pattern. Conversely, HII-DPO accurately describes the scene without relying on linguistic heuristics.

**LLaVA-v1.5-7B**

The image is a black and white photo of a park scene. In the foreground, there is a bench situated near a tree, providing a peaceful spot for relaxation. The bench is positioned on the left side of the image, while the tree is located towards the center. In the background, there is a **person** standing near the right edge of the image, possibly enjoying the park's atmosphere. The overall scene captures a serene moment in the park, with the black and white photo adding a timeless quality to the image.

**HII-DPO**

The image is a black and white photo of a tree trunk, which appears to be the main focus of the picture. The tree trunk is located in the middle of the image, with the surrounding area being black. The black background creates a striking contrast with the tree trunk, making it the main subject of the photo.

**LLaVA-v1.5-7B**

The image features a woman standing in a kitchen, preparing food. She is wearing a striped dress and is focused on her task. The kitchen is well-equipped with various appliances, including a refrigerator, an oven, and a microwave. There are multiple bottles scattered around the kitchen, possibly containing ingredients or beverages. A potted plant can be seen in the background, adding a touch of greenery to the space. A **chair** is also present in the room, likely for seating or additional storage.

**HII-DPO**

The image features a woman standing in a kitchen, surrounded by several jars of food. She is positioned in front of a stove, which is located near the center of the scene. The woman appears to be looking at the jars of food, possibly preparing them for cooking or storage. The jars are placed in various positions around her, with some closer to the stove and others further away. The woman's presence and the numerous jars create a sense of activity and preparation in the kitchen.

**LLaVA-v1.5-7B**

The image features a group of children gathered around a **dining table**, eagerly waiting for a man to serve them cake. The man is standing near the **table**, holding a knife and preparing to cut the cake. There are several children sitting and standing around the **table**, with some closer to the man and others further away. In addition to the cake, there are a few other items on the **table**, such as a cup and a handbag. The scene appears to be a celebration or a special occasion, with the man playing the role of a host or a father, ensuring that the children have a good time.

**HII-DPO**

The image features a man standing in front of a group of young girls, who are eagerly waiting for him to serve them cake. The man is holding a piece of cake, and the girls are gathered around him, eagerly anticipating their share. The scene appears to be a celebration or a special occasion, as the man is handing out the cake to the children.

Figure 8. A qualitative comparison of Detailed Description Generation (DDG) between the base LLaVA-v1.5-7B and HII-DPO.

**LLaVA-v1.5-7B**

**"person"**

Q: Describe this image in detail. You should only focus on the visible objects.

**HII-DPO**

The image features a large field of green trees with a black background. The trees are densely packed, creating a lush and vibrant scene. In the midst of the trees, there is a large umbrella that stands out against the black background. The umbrella is positioned in the middle of the field, drawing attention to itself amidst the greenery.

**LLaVA-v1.5-7B**

**"dining table"**

Q: Describe this image in detail. You should only focus on the visible objects.

**HII-DPO**

The image is a black and white photo of a dark room. The room appears to be empty, with no visible objects or details. The black background creates a stark contrast with the white photo, emphasizing the darkness of the room.

**LLaVA-v1.5-7B**

**"person"**

Q: Describe this image in detail. You should only focus on the visible objects.

**HII-DPO**

The image is a black and white photo of a tree near a body of water. The tree is located on the side of the road, providing a picturesque view of the water. The black and white nature of the photo adds a sense of timelessness to the scene. The tree is situated next to the water, creating a serene atmosphere.

Figure 9. Another qualitative comparison of Detailed Description Generation (DDG) between the base LLaVA-v1.5-7B and HII-DPO.